Electromagnetic turbulence suppression by energetic particle driven modes

A. Di Siena, T. Görler, E. Poli, A. Bañón Navarro, A. Biancalani, and F. Jenko
Max Planck Institute for Plasma Physics Boltzmannstr 2 85748 Garching Germany
(Dated: September 24, 2019)

In recent years, a strong reduction of plasma turbulence in the presence of energetic particles has been reported in a number of magnetic confinement experiments and corresponding gyrokinetic simulations. While highly relevant to performance predictions for burning plasmas, an explanation for this primarily nonlinear effect has remained elusive so far. A thorough analysis finds that linearly marginally stable energetic particle driven modes are excited nonlinearly, depleting the energy content of the turbulence and acting as an additional catalyst for energy transfer to zonal modes (the dominant turbulence saturation channel). Respective signatures are found in a number of simulations for different JET and ASDEX Upgrade discharges with reduced transport levels attributed to energetic ion effects.

PACS numbers: 52.65.Tt,52.35.Mw,52.35.Ra,52.35.Bj

Introduction. Being an almost ubiquitous phenomenon, turbulence with its highly stochastic and nonlinear character is a subject of active research in various fields. In magnetically confined plasma physics, it is of particular interest since it largely determines the radial heat and particle transport and thus the overall confinement. Any insight on possible reductions of the underlying micro-instabilities and/or on modifications of their nonlinear saturation mechanisms can be considered crucial on the way to self-sustained fusion power plants. A particularly interesting example is the recent experimental and numerical evidence suggesting a link between the presence of fast ions and substantial improvement of energy confinement in predominantly ITG (ion-temperature-gradient) driven turbulence [1–5]. Dedicated theoretical studies have already identified a number of possible energetic ion effects on plasma turbulence like dilution of the main ion species [1], Shafranov shift stabilization [6] and resonance interaction with bulk species micro-instabilities in certain plasma regimes [7, 8]. They furthermore contribute to the total plasma pressure and increase the kinetic-to-magnetic pressure ratio, β, which is a measure for the relevance of electromagnetic fluctuations, known to stabilize ITG modes. Such behaviour could indeed be confirmed in simulations [4, 9, 10] of JET hybrid discharges [11, 12] with substantial fast ion effects that, however, also identified an upper limit for this beneficial fast-ion-pressure effect. If the total plasma pressure exceeds a critical value, kinetic ballooning or Alfvénic ITG modes with smaller toroidal mode numbers and frequencies higher than the ITG modes are destabilized which increase particle/heat fluxes [13]. Although a possible relevance of the proximity to the onset of these modes has been noted [4, 9], their role was not investigated in more detail. All of these effects mainly affect the linear growth of the underlying micro-instability. A satisfactory explanation for the particularly strong *nonlinear* reduction in electromagnetic flux-tube simulations with fast ions [5, 10] still represents an outstanding issue. A substantially stronger nonlinear transport reduction compared to linear simulations is also found in electromagnetic studies without fast ions. Here, a theoretical model [14] has recently been proposed which suggests that electromagnetic fluctuations strengthen the nonlinear interaction between a large variety of unspecified stable and unstable modes with zonal flows (ZF) by increasing the so-called triplet correlation time. The further enhancement of this effect by fast ions was, however, not covered. This letter is therefore dedicated to fill the missing gaps and to provide - for the first time - a consistent picture of the nonlinear impact of fast ions on plasma turbulence. A new approach based on a frequency-spectral decomposition of the free-energy balance reveals that a central role is played by the nonlinear excitation of subdominant, energetic particle (EP) induced modes in regulating the turbulent energy.

Similarity of different discharges. A common picture emerges from the analysis of a number of different scenarios where improved ion-energy confinement was attributed to nonlinear electromagnetic EP effects [4, 5, 10, 15]. To provide corresponding evidence, three different examples – the JET (Carbon-Wall) L-mode discharge #73224 with both NBI and ICRH minority heating [5], the AUG H-mode discharge #31563 with ICRH heating [16] and the AUG H-mode non-inductive discharge #32305 with only NBI heating [10] – will be studied and presented in the following. The gyrokinetic analyses are performed with GENE [17] flux-tube turbulence simulations at the radial position where the bulk ion temperature profile steepens. The main plasma parameters are summarized in Tab. I - they and the numerical grid resolutions are the same as employed in Refs. [5, 10]. The only exceptions are the external $E \times B$ shearing rate, that it is set to zero and the absence of carbon impurities for the JET discharge #73224 to remove any turbulence reduction not related to nonlinear electromagnetic fast ion effects. A characteristic transition marked by a rather quick increase in the zonal flow amplitude

TABLE I. Parameters for the JET (Carbon-Wall) L-mode discharge #73224 at $\rho_{\rm tor} = 0.33$, the AUG H-mode discharge #31563 with ICRH heating at $\rho_{\rm tor} = 0.21$ and the AUG H-mode non inductive discharge #32305 at $\rho_{\rm tor} = 0.4$. Here, T denotes the temperature normalized to the electron one, $R/L_{T,n}$ the normalized logarithmic temperature and density gradients, $\hat{s}$ the magnetic shear $\hat{s} = (\rho_{\rm tor}/q)(dq/d\rho_{\rm tor})$, ν^* the electron-ion collision frequency normalized to the trapped electron bounce frequency, $\beta_e = 8\pi n_e T_e/B_0^2$ the ratio between the thermal electron and magnetic pressure and $\rho^* = \rho_s/a$ the Larmor-to-minor-radius.

JET	L-mode	#73224							
R/a	$\hat{s}$	q	T_i/T_e	R/L_{T_i}	R/L_{T_e}	R/L_{n_i}	$\beta_e(\%)$	ν^*	ρ_i^*
3.1	0.52	1.74	1.0	9.3	6.8	0.02	0.33	0.038	1/450
$n_{^3He}$	n_{fD}	$T_{^3He}/T_e$	T_{fD}/T_e	$R/L_{T_{^3He}}$	$R/L_{T_{fD}}$	$R/L_{n_{^3He}}$	$R/L_{n_{fD}}$	$\rho^*_{^3He}$	ρ^*_{fD}
0.07	0.06	6.9	9.8	23.1	3.2	1.6	14.8	1/200	1/150
AUG	H-mode	#31563							
R/a	$\hat{s}$	q	T_i/T_e	R/L_{T_i}	R/L_{T_e}	R/L_{n_i}	$\beta_e(\%)$	ν^*	ρ_i^*
3.4	0.32	1.4	1.2	14.1	8.5	1.7	0.5	0.06	1/263
$n_{^3He}$	n_{fD}	$T_{^3He}/T_e$	T_{fD}/T_e	$R/L_{T_{^3He}}$	$R/L_{T_{fD}}$	$R/L_{n_{^3He}}$	$R/L_{n_{fD}}$	$\rho^*_{^3He}$	ρ^*_{fD}
0.023	0	9.1	0	23.9	0	1.7	0	1/90	0
AUG	H-mode	#32305							
R/a	$\hat{s}$	q	T_i/T_e	R/L_{T_i}	R/L_{T_e}	R/L_{n_i}	$\beta_e(\%)$	ν^*	ρ_i^*
3.7	0.44	1.34	0.98	8.09	6.73	3.63	1.43	0.02	1/300
$n_{^3He}$	n_{fD}	$T_{^3He}/T_e$	T_{fD}/T_e	$R/L_{T_{^3He}}$	$R/L_{T_{fD}}$	$R/L_{n_{^3He}}$	$R/L_{n_{fD}}$	$\rho^*_{^3He}$	ρ^*_{fD}
0	0.14	0	7.90	0	1.39	0	4.86	0	1/100

and a substantial turbulence reduction before entering a long-term quasi-stationary state is observed in each of these studies as shown in Fig. 1. Moreover, a sticking observation concerns the existence of frequency components larger than the corresponding ITG (low frequency) ones in each of the considered scenarios, as demonstrated by the frequency spectra of the electrostatic field component presented in Fig. 1d). These modes (associated to high frequency components) agree well with the analytic prediction $\omega = v_{th,i}c_s/(2qR\sqrt{\beta_i})$ [18] for toroidal Alfvén eigenmodes (TAE) which are, however, absent in linear simulations and thus nonlinearly destabilized. Here, $v_{th,i}$ represents a dimensionless thermal velocity defined as $v_{th,i} = \sqrt{2T_i/T_e}$, $c_s = \sqrt{T_e/m_i}$ the ion sound speed and R the major radius of the device. The differences in the bulk plasma parameters (e.g. β_e, T_i/T_e, ν^*), energetic particle heating schemes (e.g. neutral beam injection and/or ion-cyclotron resonance heating) and magnetic configurations (e.g. q, $\hat{s}$, a, R/a) among the selected discharges show that this phenomenology is not limited to a single particular simulation setup but more universal. In this letter we present a detailed analysis on the impact of these high-frequency modes on the turbulent transport for the JET-like scenario described below.

Simulations: Setup and Results. The impact of the fast ions on the electromagnetic nonlinear stabilization of plasma turbulence is investigated with GENE [17] flux-tube turbulence simulations. We analyze in detail a JET-like scenario with deuterium, electrons and externally injected neutral beam deuterium described in detail in Ref. [7, 19], with a reduced safety factor of $q = 1.2$. The basic finding to be explained is displayed in Fig. 2a) where the flux surface averaged heat fluxes – normalized to $Q_{gB} = v_{th,i}\rho_i^2 n_e T_i/R_0^2$ – are shown for different values of the electron thermal to magnetic pressure ratio $\beta_e = 8\pi p_e/B_0^2$ in simulations with/without energetic particles. To better isolate the β_e impact on the fast ion related turbulence suppression, the magnetic geometry is kept fixed to the experimental one in the following analyses. The grid resolution in radial, binormal and parallel to the magnetic field line directions is $(x, y, z) = (192, 96, 32)$ points, while in the magnetic moment and parallel velocity $(\mu, v_{\shortparallel}) = (20, 32)$ points. The radial box size is $175\rho_s$ and the minimum $k_y\rho_s = 0.025$ with thermal gyroradius $\rho_s = (T_e/m_i)^{1/2}/\Omega_i$. Here, $\Omega_i = m_i c/q_i B_0$ denotes the gyro-frequency, T_i the main ion temperature, m_i the main ion mass, q_i the main ion charge, B_0 the magnetic field on axis and c is the speed of light. The flux-tube description appears justified given the small Larmor-to-minor-radius ratio of $\rho_i^* = 1/450$ for thermal ions and $\rho_{fD}^* = 1/150$ for the fast deuterium and was employed in all preceding studies on this subject [4, 5, 9, 10, 14, 15]. The energetic particles are modelled with an equivalent Maxwellian distribution function. This choice is not expected to change qualitatively the turbulence results as compared to more realistic background distribution functions. Ref. [20] considered numerical fast ion backgrounds from state-of-the-art heating codes for the same JET reference discharge #73224 as in the present manuscript. The more realistic shape of the NBI fast ion distribution was found to be rather insignificant compared to equivalent Maxwellian results. Similar findings were also found in Refs. [15, 21, 22].

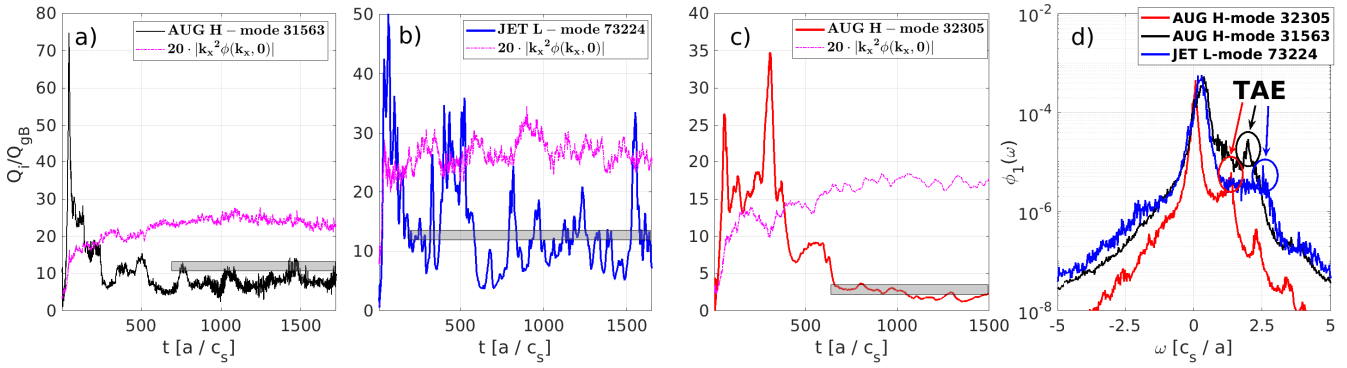

FIG. 1. Nonlinear (a-c) main ion heat flux time trace (in GyroBohm units) and zonal shearing rate (magenta lines) for the a) AUG H-mode discharge #31563, b) JET L-mode discharge #73224, c) AUG H-mode discharge #32305 and (d) k_x and z-averaged $\bar{\phi}_1$ frequency spectra for each discharge of Tab. I at the $k_y\rho_s$ corresponding to the maximum of the TAE peak, identified by analyzing the frequency spectra $\phi_1(k_y, \omega)$, i.e. $k_y\rho_s = 0.125$ for the AUG H-mode discharge #32305, $k_y\rho_s = 0.1$ for the JET L-mode discharge #73224 and $k_y\rho_s = 0.175$ for the AUG H-mode discharge #31563. For each of these discharges the dimensionless TAE frequency reads as follows, $\omega_{TAE} = 2.1$ for the AUG H-mode discharge #31563, $\omega_{TAE} = 2.5$ for the JET L-mode discharge #73224 and $\omega_{TAE} = 1.3$ for the AUG H-mode discharge #32305. The gray area denotes the experimental values within error bars normalized to $Q_{gB} = v_{th,i}\rho_i^2 n_e T_i/R_0^2$. To reduce the computational cost of the nonlinear AUG H-mode #32305 and JET L-mode #73224 simulations, the heat flux output has been calculated by the GENE code only every 500 time steps. High-frequency oscillations which occur on shorter time scales are hence not visible in this figure.

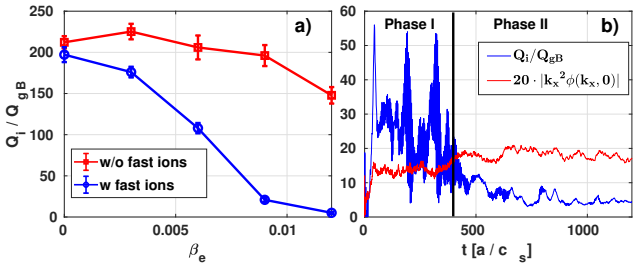

FIG. 2. Nonlinear main ion heat flux in GyroBohm units for a) different β_e and b) time trace and zonal shearing rate at $\beta_e = 0.012$ with fast ions. The vertical black line marks the time of the transition between phase I and II.

The presence of fast ions yields a substantial stabilization compared to electromagnetic simulations without, e.g. 95% at $\beta_e = 0.012$. Considering the heat flux time traces of the higher β_e simulations with strong transport reduction in more detail, two nonlinear phases can usually be observed as shown in Fig. 2b). A striking observation during the first phase are high-frequency modulations of the heat fluxes in the presence of fast ions. They can be attributed to *linearly marginally stable* EP-driven modes. Further analysis shows, analogously as the results of Fig. 1d), that they lie at the center of the toroidicity-induced gap of the SAW (shear Alfvén wave) continuous spectrum [18, 23] and exhibit the TAE frequency $\omega = v_{th,i}c_s/(2qR\sqrt{\beta_i})$ for each value of β_e and become unstable at $\beta_e \sim 0.013$. Here, $\beta_e = \beta_i T_e n_e/(T_i n_i)$. The appropriateness of a local flux-tube description to treat energetic particle modes was partially discussed in Ref. [24, 25] and can be shown to be valid for the parameters under consideration by comparison with global simulations [26]. Further signatures for the presence of these modes are given in Fig. 3a) where a Fourier transform has been applied to the gyroaveraged electrostatic potential $\bar{\phi}_1$ in the first nearly-steady state time range (phase I). Clearly, a progressive destabilization of high-frequency components with β_e can be seen (at $k_y\rho_s = 0.1$ in the plot) while no such significant difference in the electrostatic potential frequency spectra can be observed in the absence of EP in Fig. 3b). Moreover, Fig 3a) shows a corresponding reduction of the ITG peak ($\omega/[c_s/a] \sim 0.08$) from about 30% for $\beta_e = 0.003$ to about 85% for $\beta_e = 0.012$ with respect to the electrostatic limit, as the high-frequency mode is destabilized. The presence of this mode is observed in a wide spectral ($k_y\rho_s$) range which broadens with increasing β_e. For the case $\beta_e = 0.012$, for instance, high-frequency fluctuations are observed up to ITG relevant binormal mode-numbers, namely $0.025 < k_y\rho_s < 0.2$ with a maximum at $k_y\rho_s = 0.15$. During the first nonlinear phase, the energy enclosed in the TAE frequency range, namely $1.3 < \omega/[c_s/a] < 2.5$, increases from about 0% to about 30% as β_e is varied from 0 to 0.012, with a reduction in the ITG-frequency free energy content. In this phase, the zonal flow levels seem to be hardly affected by the EP presence such that the overall EP induced transport reduction remains moderate. At the beginning of a second phase, however, a significant increase in zonal component of the potential is observed. It eventually reaches a new quasi-stationary state with substantially reduced ion-scale turbulence transport, which is not subject to

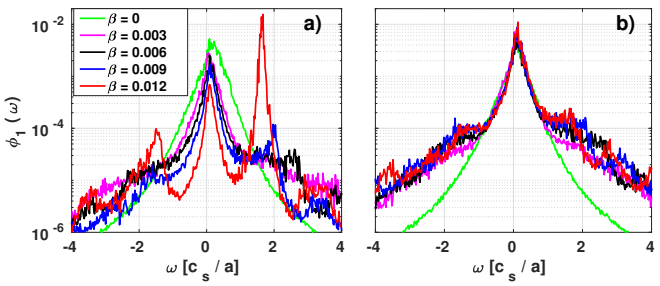

FIG. 3. Frequency spectra of $\bar{\phi}_1$ - averaged over $k_x\rho_s$ and z - for different β_e at $k_y\rho_s = 0.1$ for simulations a) with b) without fast ions in the time range $[50-340]a/c_s$. The plots share the same legend. The ITG-frequency peaks at $\omega/[c_s/a] \sim 0.08$, while the TAE frequency follows the relation $\omega/[c_s/a] = v_{th,i}/(2qR_0\sqrt{\beta_i})$ for each value of β_e. Here $\beta_i = \beta_e T_i n_i/(T_e n_e)$.

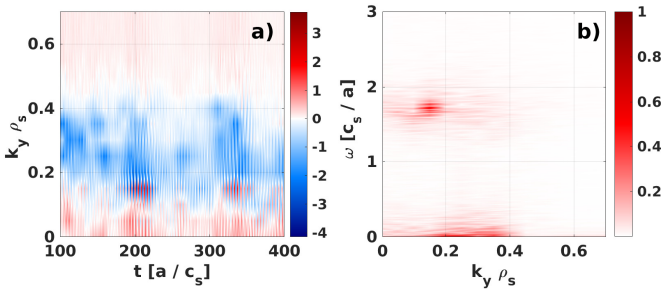

FIG. 4. Nonlinear transfer at $\beta_e = 0.012$ - averaged over $k_x\rho_s$ and z - a) in $k_y\rho_s$ and in the time domain $[100-400]a/c_s$ and b) its frequency spectra. Positive/negative values in the left plot indicate that the given wave-vector is receiving/losing energy through nonlinear coupling.

long-time secular [27, 28] zonal flow evolution. The statistical properties of the heat flux, such as skewness and kurtosis, do not deviate from the gaussian ones. It is remarked that the magnitude of the heat flux during this phase depends on the simulation physical parameters and does not imply necessarily proximity to marginality, while the nonlinear coupling to a marginally stable high-frequency mode remains an ubiquitous observation in all these scenarios.

Nonlinear energy-transfer analysis. In order to understand the phenomenology described above, the energy transfers are studied more closely, e.g., by monitoring the nonlinear mode-to-mode coupling term in the free energy balance equation [29–31]

$$\mathcal{N}_k = \sum_{k',k''} \mathcal{T}_k^{k',k''} = \sum_{s,k',k''} \Re e\Bigg\{ \int dz dv_{\shortparallel} d\mu\pi B_0 h_{1,s}^k \frac{n_s T_s}{F_{0,s}} \left[\left(\vec{k}' \times \vec{k}''\right) \cdot \frac{\vec{B}_0}{|B_0|} \right] \left(\bar{\xi}_{1,s}^{k'} g_{1,s}^{k''} - \bar{\xi}_{1,s}^{k''} g_{1,s}^{k'} \right) \Bigg\}, \quad (1)$$

with $h_{1,s}^k = f_{1,s}^k + q_s \bar{\phi}_1^k F_{0,s}/T_s$. Here, s denotes the plasma species with density n_s, temperature T_s, and charge q_s. Furthermore, $F_{0,s}$ represents the Maxwellian background, and $g_{1,s} = f_{1,s} + q_s v_{th,s} v_{\shortparallel} F_{0,s} \bar{A}_{1,\shortparallel}/T_s$ a modified distribution with the perturbed distribution function $f_{1,s}$, the thermal velocity $v_{th,s} = \sqrt{2T_s/m_s}$, the gyroaveraged parallel component of the vector potential $\bar{A}_{1,\shortparallel}$ and the field $\bar{\xi}_{1,s} = \bar{\phi}_1 - v_{th,s} v_{\shortparallel} \bar{A}_{1,\shortparallel}$. The symbol $\mathcal{T}_k^{k',k''}$ represents the nonlinear energy transfer between the modes k, k' and k''. It is a cubic function of $g_{1,k}$ and it can be expressed as a triadic nonlinear coupling between the modes k, k' and k''. Since the coupling condition $k + k' + k'' = 0$ is satisfied, the triad transfer is a symmetric function of k' and k'', i.e. $\mathcal{T}_k^{k',k''} = \mathcal{T}_k^{k'',k'}$.

Fig. 4a) shows the time evolution of the nonlinear mode-to-mode coupling term $\mathcal{N}_{k_y}(t)$ in the first nonlinear phase, summed over all radial wave-numbers for the simulation at $\beta_e = 0.012$. A significant energy transfer is observed from the ITG-relevant binormal wave-vectors $0.2 < k_y\rho_s < 0.45$ (which supply a large amount of free energy) to larger scales $0 < k_y\rho_s < 0.175$ (which absorb the free energy and channel it to zonal components). Negative (respectively positive) values of $\mathcal{N}_{k_y}$ mean that a given spectral component is giving (respectively receiving) energy through the nonlinear coupling. Although its structure is not affected by the amplitude of the magnetic fluctuations, the nonlinear energy exchange rate $\mathcal{N}(\omega)$ significantly increases with β_e. By performing a Fourier decomposition in time of $\mathcal{N}$ for each $k_y\rho_s$, fast oscillations are observed in Fig. 4b) for the binormal wave vector range $0.025 < k_y\rho_s < 0.2$ at the specific TAE mode frequency. The mode-to-mode coupling term transfers energy from ITG- to TAE-scales and is strongly enhanced by β_e. These results are consistent with the frequency peaking of the electrostatic potential of Fig. 3a).

It was noted previously that linear energy balance analyses at $k_y\rho_s = 0.1$ show that the EP-driven mode is linearly stable for $\beta_e < 0.013$, being suppressed by Landau damping mechanisms. However, as β_e increases, the curvature term contribution to the linear instability increases significantly, with a reduction of the linear damping from $\gamma_{TAE} = -0.124 c_s/a$ at $\beta_e = 0.003$ to $\gamma_{TAE} = -0.005 c_s/a$ at $\beta_e = 0.012$. As this mode becomes closer to the marginal stability, more and more energy is exchanged nonlinearly with the dominant ion-scale turbulence through mode-to-mode coupling. The interplay between nonlinear drive and damping of the EP-driven mode can be studied in detail by investigating the field component of the free energy balance [32]

$$\frac{\partial E_w^k}{\partial t} = \sum_s \Re e \left\{ \int dz dv_{\shortparallel} d\mu\pi B_0 n_s q_s \bar{\phi}_1^{k,*} \frac{\partial g_{1,s}^k}{\partial t} \right\}. \quad (2)$$

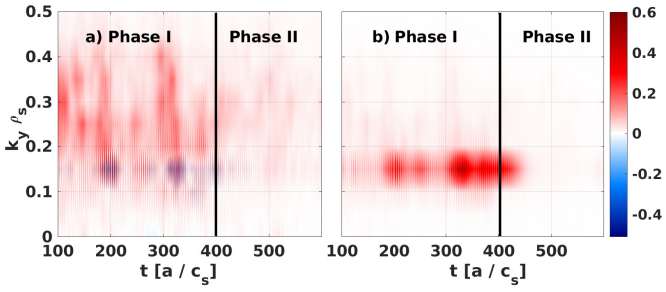

FIG. 5. Time trace of the field component of the curvature term in the free energy balance for a) thermal deuterium and b) NBI - averaged over $k_x\rho_s$ and z - for different $k_y\rho_s$ at $\beta_e = 0.012$. Positive/negative values indicate a destabilizing/stabilising contribution to the overall drive at the given wave number. The black lines mark the time of the transition between phase I and II.

This analysis is reduced to the study of the curvature term - usually destabilizing - and parallel advection - related to Landau damping mechanisms. Fig. 5 reveals that, during the first phase, significant energy is transferred from the main deuterium to the EP curvature term, which reaches amplitudes similar to the thermal species. This interaction, identified by the oscillatory pattern of Fig. 5, occurs at the TAE scale, namely $k_y\rho_s \sim 0.15$ and is modulated at the TAE frequency. Moreover, Fig. 5 shows that EPs provide the dominant contribution to the high-frequency mode, consistently with the lack of turbulence stabilization observed in their absence in Fig 2a). These results explain the progressive stabilization observed in the first phases of the nonlinear simulations with β_e. In correspondence with the second nonlinear phase, the amplitude of the main deuterium curvature term decreases significantly with non-negligible EP contributions. The latter, however, sustained only through nonlinear coupling with ITG-scales, drops at a later time - $t \sim 430a/c_s$ - as well, as a consequence of the lack of cross-scale transferred energy.

The "triad" coupling function $\mathcal{T}_k^{k',k''}$, defined in Eq. 1, is employed to investigate in detail the difference in the nonlinear interaction between EP-driven TAE and ZF in the two phases of the nonlinear simulations with energetic particles. Fig. 6 shows the triad wave-number spectra, normalized to the main ion heat flux, averaged over the time domains of the two phases for $(k_x, k_y)\,\rho_s = (0.04, 0)$, i.e. for transfer to the zonal component. No significant difference is found if the radial wave-number k_x is changed. In the first phase, the selected triplet is interacting mainly with the binormal mode numbers in the range $0.2 < k_y\rho_s < 0.4$, as can be seen in Fig. 6a). At this scale, the ITG-drive peaks and the time-averaged EP-driven mode contribution is negligible, as confirmed by the frequency decomposition of the time trace of the overall triplet. In the first nonlinear phase, the TAE mode is not interacting significantly with zonal modes. However, as the energy is nonlinearly transferred from ITG to TAE scales, the amplitude of the EP-driven modes increases significantly and ZFs are more and more affected by the presence of these modes. In the second nonlinear phase, the whole energy transfer to the specific triplet occurs through the wave-vector $k_y\rho_s = 0.15$, where the TAE mode is dominant and it overcomes the thermal ITG contribution. The energy exchange increases by a factor of ~ 30. The TAE mode therefore acts as an additional mediator of plasma turbulence, catalyzing energy transfer to zonal modes, strongly affecting the standard paradigm

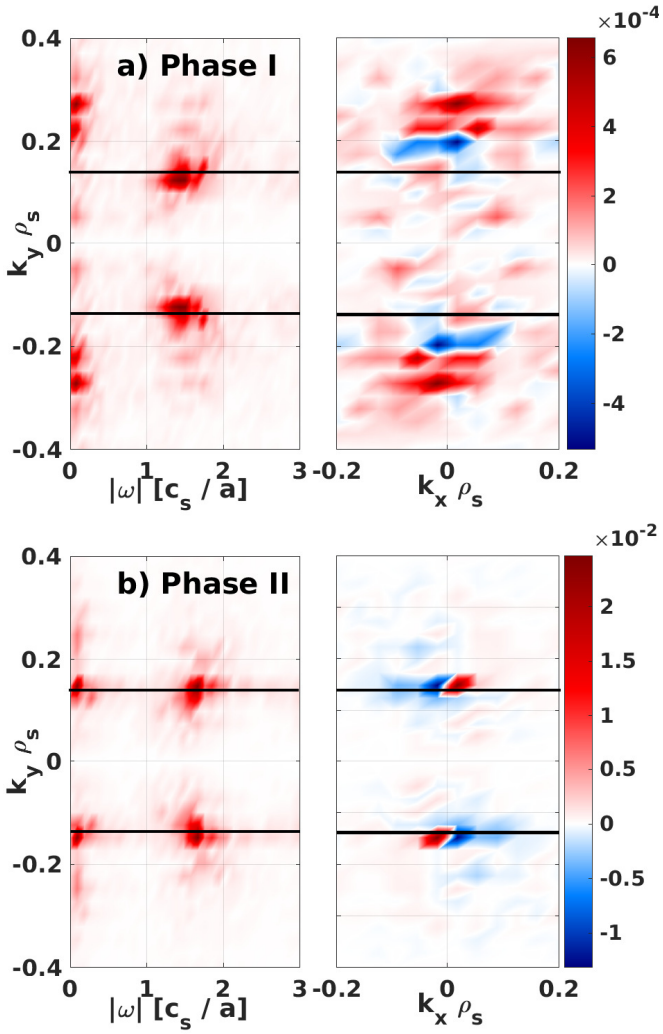

FIG. 6. Triad energy transfer to the zonal component normalized to the main deuterium heat flux as function of (ω, k_y) deep in the a) first ($t = 165 - 245\,a/c_s$) and b) second phase ($t = 470 - 550\,a/c_s$). The black line denotes the dominant TAE scale $k_y\rho_s = 0.15$. Positive/negative values indicate that a given wave-vector is receiving/losing energy through nonlinear coupling with the resonant modes. Note the difference in the colorbar, i.e. in the amplitudes in the two phases.

of ZF/ion-scale-turbulence interaction [29, 33]. It should be mentioned at this point that experimental signatures of the nonlinear coupling between ion-scale turbulence and high-frequency Alfvénic instabilities has also been recently observed at HL-2A in a strong NBI heated discharge [34]. The physical mechanism described in this letter may very well open ways for new physical interpretations of more general turbulent systems well beyond the scenarios which involve energetic ions and magnetically confined plasmas [35–39]. In particular, similar nonlinear effects might be observed each time subdominant modes approach the marginal stability threshold and are allowed to couple with both the dominant instabilities and the stable modes acting as main saturation players. Particularly strong nonlinear reductions have, e.g., also been found in the absence of energetic ions in transitions from trapped-electron to ITG modes [40] and are an obvious subject for further investigations along these lines.

Conclusions. The intriguing and particular strong transport reduction in the presence of fast ions observed in several scenarios could - for the first time - be explained by their ability to trigger marginally stable modes which are nonlinearly excited and act as a catalyst for the main turbulence saturation mechanisms. These findings are not restricted only to TAEs and similar results could be observed each time the linear excitation threshold of subdominant modes (e.g. BAE, KBM, EPM) is approached. While already being highly relevant to plasma physics with strong heating, this study may furthermore motivate deliberate "design" of marginally stable modes in order to exploit their capability as mediators boosting nonlinear saturation mechanisms such as zonal flows.

In the case discussed in this paper – a strongly NBI-heated JET discharge with fast ion related temperature profile steepening – a two-phase process could be observed in nonlinear gyrokinetic simulations and analyzed with new spectral analyses techniques. The fast ions provide linearly marginally stable TAE modes which are nonlinearly excited by an energy redistribution from ITG to TAE spatio-temporal scales. As a result, lower transport levels corresponding to the net reduction of the ITG drive can be observed. If sufficiently populated, the fast ion modes furthermore start to increasingly affect the ZF levels which marks a second phase in the simulations. During this phase, the energy being nonlinearly transferred to zonal modes undergoes a substantial increase in magnitude and is modulated at the TAE frequency. The increase in ZF levels directly impacts the ion-scale turbulence, strongly suppressing heat/particle fluxes. This in turns lowers the nonlinear drive of the EP modes. The system finally finds an equilibrium at a much reduced transport level. This mechanism with possibly high relevance to future plasma performance predictions is not restricted to a specific scenario, but could also be identified in different JET and ASDEX Upgrade discharges with strong heating and moreover seems to be consistent with recent experimental and analytic studies [34, 41].

The simulations presented in this work were performed at the Cobra HPC system at the Max Planck Computing and Data Facility (MPCDF), Germany. Furthermore, we acknowledge the CINECA award under the ISCRA initiative, for the availability of high performance computing resources and support. The authors would like to thank N. Bonanomi, J. Citrin, H. Doerk, Ph. Lauber, P. Manas, P. Mantica, M. J. Pueschel, K. Stimmel, P. W. Terry, D. Zarzoso, and A. Zocco for all the stimulating discussions, useful suggestions and comments.

[1] G. Tardini, J. Hobirk, V. G. Igochine, C. F. Maggi, P. Martin, D. McCune, A. G. Peeters, A. C. C. Sips, A. Stäbler, J. Stober, and ASDEX Upgrade Team, Nucl. Fusion **47**, 280 (2007).
[2] M. Romanelli, A. Zocco, F. Crisanti, and JET Contributors, Plasma Phys. Controlled Fusion **52**, 045007 (2010).
[3] C. Holland, C. C. Petty, L. Schmitz, K. H. Burrell, G. R. McKee, T. L. Rhodes, and J. Candy, Nucl. Fusion **52**, 114007 (2012).
[4] J. Citrin, J. Garcia, T. Görler, F. Jenko, P. Mantica, D. Told, C. Bourdelle, D. R. Hatch, G. M. D. Hogeweij, T. Johnson, M. J. Pueschel, and M. Schneider, Plasma Phys. Controlled Fusion **57**, 014032 (2015).
[5] J. Citrin, F. Jenko, P. Mantica, D. Told, C. Bourdelle, J. Garcia, J. W. Haverkort, G. M. D. Hogeweij, T. Johnson, and M. J. Pueschel, Phys. Rev. Lett. **111**, 155001 (2013).
[6] C. Bourdelle, G. T. Hoang, X. Litaudon, C. M. Roach, and T. Tala, Nucl. Fusion **45**, 110 (2005).
[7] A. Di Siena, T. Görler, H. Doerk, E. Poli, and R. Bilato, Nucl. Fusion **58**, 054002 (2018).
[8] A. Di Siena, T. Görler, E. Poli, R. Bilato, H. Doerk, and A. Zocco, Physics of Plasmas **26**, 052504 (2019).
[9] J. Garcia, C. Challis, J. Citrin, H. Doerk, G. Giruzzi, T. Görler, F. Jenko, P. Maget, and JET Contributors, Nucl. Fusion **55**, 053007 (2015).
[10] H. Doerk, A. Bock, A. Di Siena, E. Fable, T. Görler, F. Jenko, J. Stober, and The ASDEX Upgrade Team, Nucl. Fusion **58**, 016044 (2018).
[11] P. Mantica, D. Strintzi, T. Tala, C. Giroud, T. Johnson, H. Leggate, E. Lerche, T. Loarer, A. G. Peeters, A. Salmi, S. Sharapov, D. Van Eester, P. C. de Vries, L. Zabeo, and K.-D. Zastrow, Phys. Rev. Lett. **102**, 175002 (2009).
[12] P. Mantica, C. Angioni, C. Challis, G. Colyer, L. Frassinetti, N. Hawkes, T. Johnson, M. Tsalas, P. C. de Vries, J. Weiland, B. Baiocchi, M. N. A. Beurskens, A. C. A. Figueiredo, C. Giroud, J. Hobirk, E. Joffrin, E. Lerche, V. Naulin, A. G. Peeters, A. Salmi, C. Sozzi, D. Strintzi, G. Staebler, T. Tala, D. Van Eester, and T. Versloot, Phys. Rev. Lett. **107**, 135004 (2011).
[13] M. J. Pueschel and Jenko, Phys. Plasmas **17**, 102310 (2010).
[14] G. G. Whelan, M. J. Pueschel, and P. W. Terry, Phys. Rev. Lett. **120**, 175002 (2018).
[15] N. Bonanomi, P. Mantica, A. Di Siena, E. Dela-

bie, C. Giroud, T. Johnson, E. Lerche, S. Menmuir, M. Tsalas, D. Van Eester, and JET Contributors, Nuc. Fusion. **58**, 056025 (2018).
[16] M. J. Mantsinen, R. Bilato, V. V. Bobkov, A. Kappatou, R. M. McDermott, M. Nocente, T. Odstrčil, G. Tardini, M. Bernert, R. Dux, T. Hellsten, P. Mantica, M. Maraschek, S. K. Nielsen, J.-M. Noterdaeme, J. Rasmussen, F. Ryter, M. Stejner, J. Stober, M. Tardocchi, the ASDEX Upgrade Team, and the EUROfusion MST1 Team, AIP Conf. Proc. **1689**, 030005 (2015).
[17] F. Jenko, W. Dorland, M. Kotschenreuther, and B. N. Rogers, Phys. Plasmas **7**, 1904 (2000).
[18] L. Chen and F. Zonca, Rev. Mod. Phys. **88**, 015008 (2016).
[19] R. Bravenec, J. Citrin, J. Candy, P. Mantica, T. Görler, and JET Contributors, Plasma Phys. Controlled Fusion **58** (2016), 10.1088/0741-3335/58/12/125018.
[20] A. Di Siena, T. Görler, H. Doerk, R. Bilato, J. Citrin, T. Johnson, M. Schneider, E. Poli, and JET Contributors, Phys. Plasmas **25**, 042304 (2018).
[21] C. Angioni and A. G. Peeters, Phys. Plasmas **15**, 052307 (2008).
[22] G. J. Wilkie, I. G. Abel, E. G. Highcock, and W. Dorland, J. Plasma Phys. **81** (2015), 10.1017/S002237781400124X.
[23] C. Z. Cheng and M. S. Chance, Physics of Fluids B **29**, 3695 (1986).
[24] E. M. Bass and R. E. Waltz, Phys. Plasmas **17**, 112319 (2010).
[25] H. Sheng, R. E. Waltz, and G. M. Staebler, Phys. Plasmas **24**, 072305 (2017).
[26] A. Di Siena and et al. in preparation, .
[27] F. Rath, A. G. Peeters, R. Buchholz, S. R. Grosshauser, P. Migliano, A. Wikl, and D. Strintzi, Phys. Plasmas **23**, 052309 (2016).
[28] A. G. Peeters, F. Rath, R. Buchholz, Y. Camenen, J. Candy, F. J. Casson, S. R. Grosshauser, W. A. Hornsby, D. Strintzi, and A. Wikl, Phys. Plasmas **23**, 082517 (2016).
[29] M. Nakata, T.-H. Watanabe, and H. Sugama, Phys. Plasmas **19**, 022303 (2012).
[30] S. Maeyama, Y. Idomura, T.-H. Watanabe, M. Nakata, M. Yagi, N. Miyato, A. Ishizawa, and M. Nunami, Phys. Rev. Lett. **114**, 255002 (2015).
[31] S. Maeyama, T.-H. Watanabe, and A. Ishizawa, Phys. Rev. Lett. **119**, 195002 (2017).
[32] A. Bañón Navarro, P. Morel, M. Albrecht-Marc, D. Carati, F. Merz, T. Görler, and F. Jenko, Phys. Plasmas **18**, 092303 (2011).
[33] P. H. Diamond, S. H. Itoh, K. Itoh, and T. S. Hahm, Plasma Phys. Controlled Fusion **47**, R35?R161 (2005).
[34] W. Chen, M. Jiang, Y. Xu, P. W. Shi, L. M. Yu, X. T. Ding, Z. B. Shi, X. Q. Ji, D. L. Yu, Y. G. Li, Z. C. Yang, W. L. Zhong, Z. Y. Qiu, J. Q. Li, J. Q. Dong, Q. W. Yand, Y. Liu, L. W. Yan, M. Xu, and X. R. Duan, Nuc. Fusion. **57**, 114003 (2017).
[35] A. T. Lin, K. R. Chu, C. C. Lin, C. S. Kou, D. B. McDermott, and N. C. Luhmann Jr, Int. J. Electron. **72**, 873 (1992).
[36] Q. S. Wang, D. B. McDermott, and N. C. Luhmann, Phys. Rev. Lett. **75**, 23 (1995).
[37] W. van Saarloos, Phys. Rev. D **39**, 6367 (1989).
[38] R. G. Cai, X. He, H. F. Li, and H. Q. Zhang, Phys. Rev. D **84**, 046001 (2011).
[39] S. S. Gubser, Phys. Rev. D **78**, 065034 (2008).
[40] F. Merz and F. Jenko, Nucl. Fusion **50**, 054005 (2010).
[41] A. M. Balk, Phys. Rev. E. **98**, 062208 (2018).